Eur. Phys. J. Plus (2024) 139:347
https://doi.org/10.1140/epjp/s13360-024-05096-0

THE EUROPEAN PHYSICAL JOURNAL PLUS

Regular Article

Evaluation of RESRAD-BUILD and MicroShield codes for the simulation of small accident scenarios in nuclear medicine therapy patients' rooms

Giorgia Stendardo[1,2], Claudio Andenna[3], Paola Fattibene[1,a], Paolo Ferrari[4], Cristina Nuccetelli[5], Gennaro Venoso[5], Carmine Zicari[3]

[1] Core Facilities, Istituto Superiore Di Sanità, Viale Regina Elena 299, 00161 Rome, Italy
[2] National Center for Innovation Technology in Public Health, Istituto Superiore di Sanità, Viale Regina Elena 299, 00161 Rome, Italy
[3] DIT, INAIL, Via Torraccio Di Torrenova 7, 00133 Rome, Italy
[4] Radiation Protection Institute, ENEA, Via Martiri Di Monte Sole 4, 40129 Bologna, Italy
[5] National Center for Radiation Protection and Computational Physics, Istituto Superiore Di Sanità, Viale Regina Elena 299, 00161 Rome, Italy

Received: 5 August 2023 / Accepted: 11 March 2024

Abstract Computational methods in nuclear medicine therapy can be very useful for estimating the external dose in non-routine situations when conventional dosimeters may be inadequate or unavailable. Monte Carlo techniques provide the most accurate approach when it comes to model complex scenarios, but they are time and machine resource consuming. In this work we explore the alternative of using two fast and interactive deterministic codes, RESRAD-BUILD and MicroShield, primarily designed for radiation protection purposes, to calculate the dose in small, simple accidental scenarios, and benchmarked them with two Monte Carlo simulation tools, MCNP6 and Geant4. The absorbed dose rate in air computed by RESRAD-BUILD and compared to MicroShield showed a mean ratio of 1.01 ± 0.04 for Lu-177 and 0.99 ± 0.04 in the case of a point source and within 25% for an area source. When compared to MCNP6 and Geant4, the results revealed an overall agreement among the codes, showing a deviation below 30% in most cases, with a few exceptions that are discussed. We also propose a preliminary approach for easy modeling of patient's organs to calculate the external dose from routine therapies with deterministic methods. The suitability and limitation of these models are presented and discussed for some common applications.

1 Introduction

The integration of computational dosimetry with more advanced methods of computer simulation, artificial intelligence and computer vision can provide new approaches to near real-time computational dosimetry [1]. These approaches rely on vision tools to track the movements of workers, which are then integrated into computed radiation field maps. By using computational methods to calculate the dose in air for typical accident scenarios, and reconstructing the position of the worker's body in time and space, it is possible to calculate the dose as the worker moves through the radiation field. The potential of this approach is that it can provide tools for real-time dosimetry of workers, especially when conventional dosimeters—active or passive, normally used for monitoring—are unresponsive, inadequate or simply considered uncomfortable to wear. Real-time computational dosimetry is therefore a tool that can complement, but not necessarily replace, passive or active dosimeters.

The well-known limitation of passive dosimeters is that they do not allow the conditions and time of an acute event, such as an accident, to be traced. Active dosemeters, on the other hand, have advantages such as direct measurement of dose, and an alarm if a dose threshold is exceeded. However, both types of dosimeter provide the dose at a single point on the surface of the body and are inadequate where the worker's body is inhomogeneously or partially exposed or where the source is shielded by obstacles. Real-time computational dosimetry has the ability to reconstruct a realistic exposure scenario that includes sources, obstacles and person bodies, and to calculate the dose at different points on the body surface. These features are particularly important for dose estimation in non-homogeneous exposure scenarios and can provide a more accurate dose to sensitive organs.

An early application of real-time computational dosimetry in the hospital environment was the estimation of personnel dose in interventional radiology procedures [2] and could be extended to situations where conventional computational dosimetry has already been well established, such as for medical rescuers treating contaminated victims during radiation emergencies [3] or for rapid dose estimation in industrial radiation accidents [4]. In our laboratory, we are developing an application to reconstruct the external dose to healthcare workers during accidents and near-misses in nuclear medicine departments [5, 6]. Real-time computational dosimetry is

[a] e-mail: paola.fattibene@iss.it (corresponding author)

Published online: 24 April 2024

well suited in these cases because both interventional radiology and nuclear medicine present different scenarios of non-homogeneous worker exposure.

One of the critical aspects of this type of approach is the time required to calculate the radiation maps. These are typically calculated using Monte Carlo codes, which are time-consuming for both the machine and the operator. Artificial intelligence could be used to speed up Monte Carlo dose calculations, but these techniques are not yet widely available for use or operation by everyone. Alternatively, deterministic codes, which are faster than Monte Carlo, could be used to calculate radiation maps when it is necessary to quickly simulate new scenarios within real-time computational dosimetry systems. We therefore calculated dose rates using two deterministic codes, RESRAD-BUILD [7] and MicroShield (Grove Software) [8], and compared the results with Monte Carlo codes (Geant4 and MCNP6) as benchmarks. The verification of RESRAD-BUILD with the MCNP6 transport code is already available for high energy gamma emitters such as Co-60 and Mn-54 [9]. Several works have also compared the MicroShield code with Monte Carlo methods in the design and calculation of radiation shielding [10, 11]. In this work, two radioactive isotopes were considered that are particularly relevant for their use in nuclear medicine therapy, namely I-131 and Lu-177.

In this work, the codes were tested on simplified small accident scenarios, such as the dropping of an iodine tablet (simulated by a point source) and a liquid spill (simulated by an area source) in the absence or presence of a patient (simulated by a phantom MIRD) without internal radioactivity. Routine therapy scenarios with a patient treated as a radiation source were also considered, as a nuclear medicine therapy accident is likely to occur in the presence of a patient. In addition, a radiation map describing an accident should also include external exposure due to radioactivity in the patient's body.

2 Methods and materials

2.1 Scenarios

The comparison between the codes was made considering first two simplified accident scenarios that may occur in a protected room for nuclear medicine therapy that are the fall and the spillage of a material containing radioactivity (e.g., spillage of radiopharmaceutical solution during administration, accidental leakage of urine from the bag, vomiting of the patient, dropping of an iodine tablet). These scenarios were simulated as a point source (to describe the dropping of the tablet) and an area source (the spillage of a fluid) of I-131 or Lu-177, two common radionuclides used for radiopharmaceuticals in nuclear medicine. The maximum beta electron energy for Lu-177 is about 497 keV and for I-131 about 606 keV, corresponding to an extrapolated beta range in air of about 1.3 and 1.7 m, respectively [22].

In the second place, standard therapy scenarios, where the source is a patient's organ with no accidental event, were simulated. Thyroid and stomach for I-131 and stomach, liver and spleen for Lu-177 were considered, respectively, as some of the organs in which these radionuclides are most concentrated [12, 13].

All the simulations were performed considering a 4×4 square meter room (walls, floor, ceiling bed and the other possible structures in the room were not simulated).

RESRAD-BUILD and MicroShield were tested in the point source and the area source scenarios and, as a preliminary approach, for standard therapy scenarios (i.e., considering a patient's organ as a source). Monte Carlo codes were used as a benchmark for deterministic codes. The reason for using two Monte Carlo codes is that both were used with restrictions to manage the computation time. A summary of all the simulations performed is shown in Table 1.

2.2 Geant4

Geant4 [14–16] is a free object-oriented software package written in C + + for the simulation of the passage of particles through the matter. The room was simulated as a square cube filled with air, completely voxelized with 2-cm side cubic voxels, as a compromise between the cost of computational resources and a good granularity of dose distributions. The isotopes' sources were located inside both some organs of the phantom and in an external volume to simulate the different scenarios described in 2.1. The electromagnetic physics was simulated by activating the package "G4EmPenelopePhysics," while the radioactive decay physics was activated using

Table 1 Exposure scenarios considered for each radionuclide

Scenario	Radionuclide	Source type	Organ source
Accidental dropping of a pill on the bed	I-131	Point	–
Accidental vomiting on the bed	I-131	Area	–
Standard therapy	I-131	Volume	Thyroid, stomach
Accidental spillage from a syringe on the bed	Lu-177	Point	–
Accidental rupture of the urine bag on the floor	Lu-177	Area	–
Standard therapy	Lu-177	Volume	Stomach, spleen, liver

"G4Radioactivation." Once the selected isotope is set as primary particles, Geant4 internally simulates its decay using its internal data tables. By this method the result is the cumulative dose rate from the electron and photon components; therefore, in this work Geant4 results were used as a benchmark of the deterministic results only for distances from the source higher than the extrapolated range of the beta decay, where the electron component is null. For I-131, beta emission was described by six maximum energies, with the two more intense at 606 keV (89.6%) and 334 keV (7.2%), while the main peaks of the gamma spectrum considered were 364.5 keV (81.7%), 637 keV (7.1%) and 284 keV (6.1%). For Lu-177, beta emission was described by four maximum energies, with the two more intense at 497 keV (79%) and 384 keV (9%), while the main peaks of the gamma spectrum considered were 208 keV (11%) and 113 keV (6.4%). The cuts limits were set to 0.1 mm for all the simulated particles (electron, proton, positron and gamma). The number of primary stories was set in each scenario so as to give stable results and will be reported in figure captions.

2.3 MCNP6

MCNP6 (Monte Carlo N–Particle Transport Code System) [17] is a multi-purpose transport code that can treat different particles as neutrons, photons, electrons, ions and other elementary particles in three-dimensional complex geometries.

In our simulations the dose was computed inside air spheres of 5 cm diameter with centers spaced 10 cm. The contribution from photons and beta electrons was calculated separately. Therefore the photon component of the dose rate (herein called MCNP6_photons) was used for comparison with the deterministic codes, whereas the total beta electron and photon (herein called MCNP6) was used as a comparison with Geant4. The isotopes' decay was simulated by generating the electrons and the gamma particles according to their energies and abundance in the isotopes' emissions. Both the radioisotopes of interest emit photons and beta, which were treated separately. In the case of I-131, the main 18 energy peaks of the gamma spectrum were considered, with a calculated mean spectrum energy of 378 keV. Since a beta continuous spectrum is not acceptable in standard MCNP6 syntax, beta emission was discretized in 44 bins, from 1 to 568 keV. The mean energy of the resulting spectrum was 177 keV. In the case of ^{177}Lu, the main photon emissions of 113 keV (6.4%) and 210 keV (11%) were considered. The beta spectrum was approximated as a discrete source of 20 bins, from 12.5 keV to 484.7 keV with a mean energy of 133 keV. The number of primary stories was 4×10^7 for photons and $3.5ex10^8$ for electrons. The population percent standard deviation was calculated by the code and was of the order of (or less than) 5% for both radionuclides. This value was used as the uncertainty associated with the absorbed dose rate in the air spheres.

2.4 RESRAD-BUILD

RESRAD-BUILD is part of the RESRAD family of codes, developed at Argonne National Laboratory [7]. The code uses pathway analysis to evaluate radiation exposure and associated risks. RESRAD-BUILD is a deterministic code designed to model radionuclide release and transport in indoor environments for the evaluation of the potential radiological dose and risk incurred by an individual (human receptor) who works or lives in a contaminated building. The code enables to set building parameters (e.g., size of the room), receptor parameters (e.g., midpoint location), source parameters (e.g., location of centroid of source, geometry and radionuclide concentration) and provides four geometries to characterize a radiation source: point, line, area and volume, in which radionuclides are homogeneously distributed (CAPTIONS Fig. 1). The geometry can be set as circular or rectangular for area and parallelepiped or cylindrical for volume sources. The code has a user-friendly interface and takes up a short computational time (less than 1 min in most of the simulations performed).

Two direct external exposure models based on the geometrical type of sources are used in RESRAD-BUILD. The model for point and line contamination is a dose integral method. The model for area and volume sources is based on an infinite slab source, with correction factors, estimated using the point-kernel method, to account for the geometry and finite dimensions of actual sources.

The output is expressed in terms of the effective dose. To compare the results with the other computational methods used in this work, the effective dose rate was converted into absorbed dose in air. The orientation of the receptor has an impact on the effective dose. Therefore, considering that in most situations the receptor is moving around and is not in a fixed position facing the source, RESRAD-BUILD uses the external dose conversion factors from absorbed dose in air to effective dose (Sv/Gy) for rotational orientation taken from ICRP-74 [18]. In rotational geometry, the body is irradiated by a parallel beam from a direction orthogonal to the long axis of the body, which rotates at a uniform rate around the long axis. Even if a more recent ICRP Publication, ICRP-116 [19] has updated these factors, in the range of gamma energies emitted by Lu-177 and I-131 the differences between ICRP-116 and ICRP-74 are generally less than 1%. Therefore, RESRAD-BUILD effective dose was converted into absorbed dose in air by using ICRP-116 dose conversion factors. We assumed a mean yield-weighted energy of 173 keV for Lu-177 photons, corresponding to a conversion factor of 0.81 and an energy of 364 keV for I-131 photons, corresponding to a conversion factor of 0.86.

2.5 MicroShield

MicroShield is a commercial software from Grove Engineering, Inc. [8], for photon/gamma ray shielding and dose assessment. It is widely used for designing shields, estimating source strength from radiation measurements and minimizing exposure to people. MicroShield is fully interactive, allowing the definition of geometry and source in a simple interface (Fig. 2). It uses the point-kernel

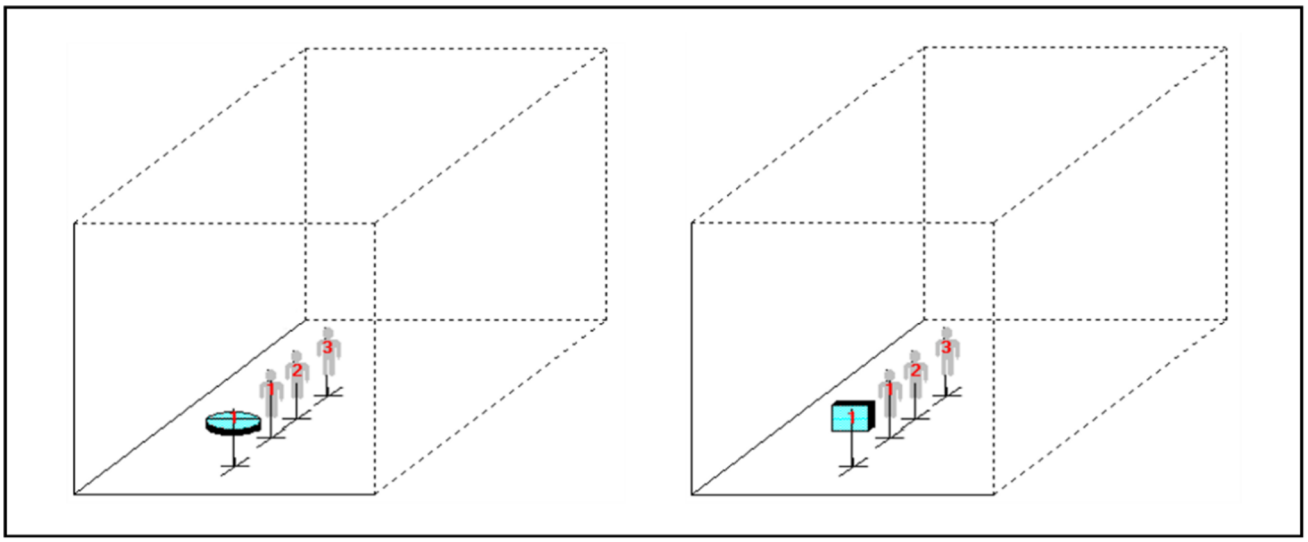

Fig. 1 Geometry of the room (4 m side) used for RESRAD-BUILD simulations. The area (left) and volume (right) sources are shown. Three receptors at 0.5, 1 and 1.5 m from the source center are also shown

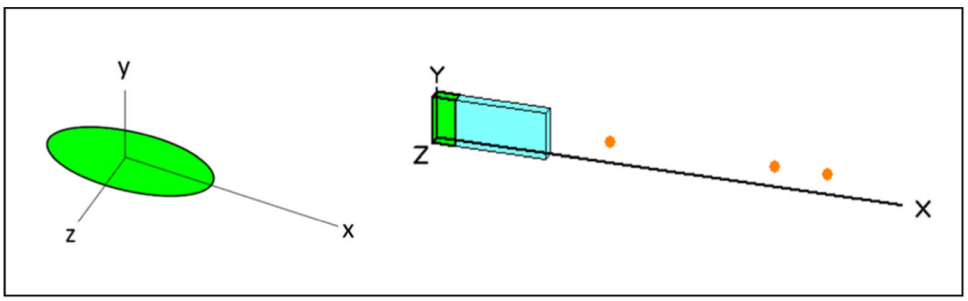

Fig. 2 Example of a geometry for a circular area source (left) and a parallelepiped volume source with a shield of water material (right) used in MicroShield, indicating the reference axis used for the simulations. The orange circles in the figure on the right indicate the calculation points

method for assessing the absorbed dose in air for each radionuclide, taken from different radionuclide transformation databases including the ICRP-107, which is the one used in calculations [20]. The photon energies have been grouped in 20 bin intervals, with main energies of 208 keV (11%) and 113 keV (6.4%) for Lu-177, and 400 keV (82%) and 600 keV (7.4%) for I-131.

In this work MicroShield was used to simulate small accident scenarios and test standard therapy scenarios simulations as a second deterministic code. The dose in air computations was carried out in the same geometries and at the same locations as those used for the RESRAD-BUILD code.

2.6 Patient and organ simulation

When using Monte Carlo codes, the patient is simulated with the Medical Internal Radiation Dose (MIRD) Committee phantom, which is a heterogeneous mathematical representation of the human body.

In this work we used the male adult model centered within a parallelepiped of air with the dimensions of the room. For Geant4, the MIRD phantom was based on the 'human-phantom' of the Geant4 advanced examples. The materials of the different organs simulated in the MIRD phantom were "G4_TISSUE_SOFT_ICRP," "G4_BONE_COMPACT_ICRU" and "G4_LUNG_ICRP" with the given densities except for the lung material for which 0.386 g/cm^3 was used. In MCNP6, the MIRD anthropomorphic male model is a part of the given standard libraries.

With RESRAD-BUILD and MicroShield, the patient's organs as sources of gamma radiation were simulated by simple parallelepiped volume sources of Lu-177 or I-131 to model thyroid, spleen, stomach and liver (CAPTIONS Figs. 1 and 2). Between each source and the human receptor, a shield of water was placed to emulate the tissues surrounding the organs. All the parallelepiped sizes and shield thicknesses were chosen to match organ dimensions and location in the MIRD phantom as much as possible.

A counterclockwise reference system was used in all codes. Where the phantom is present, this reference system is centered in the phantom with the Z-axis as the phantom central axis extending from the feet to the head, as shown in Fig. 3. The same reference system was used for the simulations of the area source without the phantom, but in these cases centered in the area source (Figs. 1 and 2).

A summary of the main parameters used in this paper for the four codes is given in Table 2.

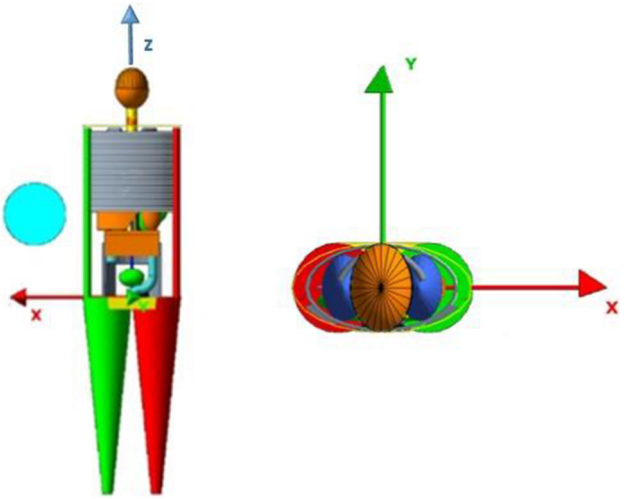

Fig. 3 Front (left part of the figure) and top (right part) view of the male MIRD phantom with the spill of water as a source. The neck and the outer layers of the head and trunk are not shown. The counterclockwise reference system used in this paper is shown

Table 2 Main parameters used for the four codes in this paper

Software	Output dose quantity	Dose target	Organ simulation
Geant4	Air kerma	2-cm side cubic voxels	MIRD phantom based on the human phantom of Geant4 advanced examples
MCNP6	Air kerma	5-cm-diameter spherical voxels	MIRD anthropomorphic male model
RESRAD-BUILD	Effective dose	Midpoint of receptor	Simple geometric sources (point, rectangular or circular area, parallelepiped or cylindrical volume)
MicroShield	Absorbed dose in air	Point in air	Simple geometric sources (point, rectangular or circular area, parallelepiped or cylindrical volume)

2.7 Reported dose quantities and associated uncertainties

Regardless of the output dose quantities of the codes, the results will be given in terms of absorbed dose rate in air per unit of activity (μGy/h/GBq), as a function of the radial distance, r, from the center of the source (unless otherwise stated in the text). In the text we will use the short-term "dose rate" to refer to this quantity and we will use $\dot{D}(r)$.

The comparison between $\dot{D}(r)$ computed by the different codes will be discussed as dose rate ratios. For example with respect to MCNP6, the dose rate ratio, *DRR(r)*, was calculated using the following expression:

$$\mathrm{DRR}(r) = \frac{\dot{D}_{\mathrm{code}}(r)}{\dot{D}_{\mathrm{MCNP6}}(r)} \tag{1}$$

The uncertainty in DRR*(r)*, *u*, will be calculated by the propagation rule:

$$u^2(\mathrm{DRR}(r)) = \left[\left(\left(\frac{u\left(\dot{D}_{\mathrm{code1}}(r)\right)}{\dot{D}_{\mathrm{code1}}(r)}\right)^2 + \left(\frac{u\left(\dot{D}_{\mathrm{code2}}(r)\right)}{\dot{D}_{\mathrm{code2}}(r)}\right)^2\right)\left(\frac{\dot{D}_{\mathrm{code1}}(r)}{\dot{D}_{\mathrm{code2}}(r)}\right)^2\right] \tag{2}$$

The uncertainty in the MCNP6 dose rate, $u\left(\dot{D}_{MCNP6}(r)\right)$, was 5% of the dose rate, as explained in 2.3. For Geant4, the number of primary histories was chosen to give stable results for most scenarios. In cases where the scatter of the data was high (e.g., when the phantom body caused radiation absorption), the standard deviation calculated from ten adjacent points was used to represent the uncertainty associated with the dose rate. No uncertainty was associated with the deterministic RESRAD-BUILD and MicroShield codes.

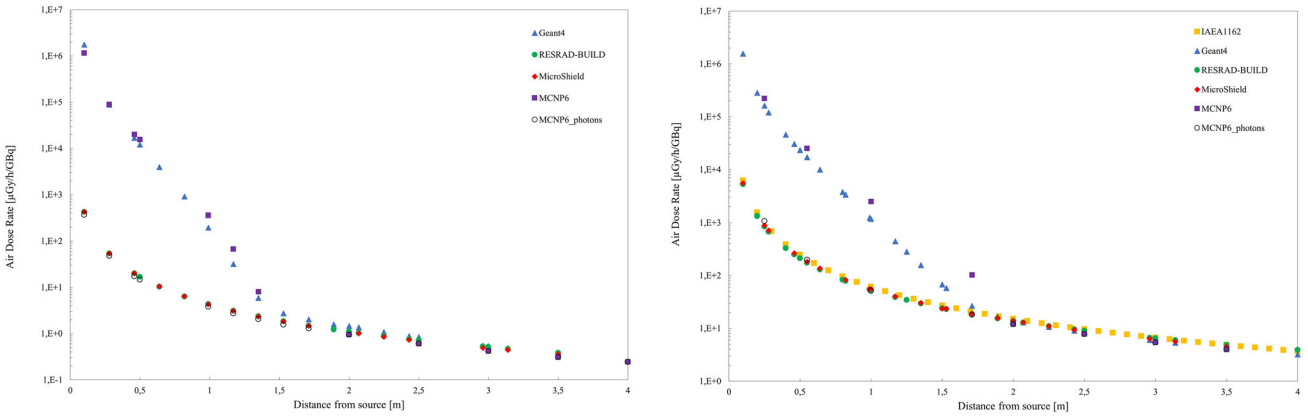

Fig. 4 Profile of dose rate as a function of the distance from the point source for Lu-177 (left) and I-131 (right)

Table 3 Comparison of dose rate in the point source geometry for Lu-177 and I-131 at different distances from the source, calculated by Geant4, MCNP6. RESRAD-BUILD and MicroShield

	Lu-177								I-131							
	0.25 m	0.55 m	1.0 m	1.7 m	2.0 m	2.5 m	3.0 m	3.5 m	0.25 m	0.55 m	1.0 m	1.7 m	2.0 m	2.5 m	3.0 m	3.5 m
Code	*Air dose rate [μGy/h/GBq]*															
Geant4	87,464	12,079	196	2	1.4	0.8	0.5	0.4	161,026	17,140	1172	26.5	14.0	8.4	5.9	4.3
MCNP6	88,857	15,508	359	1.3	0.95	0.6	0.4	0.3	220,667	25,171	2477	102	12	7.8	5.4	4.0
MCNP6_photons	48.0	14.7	3.8	1.3	0.95	0.6	0.4	0.3	843	187	51	18	12	7.8	5.4	4.0
Resrad Build	53.7	16.9	4.3	1.5	1.1	0.7	0.5	0.4	843	174	53.2	18.9	13.7	9.0	6.4	4.9
MicroShield	54.5	18	4.3	1.5	1.1	0.7	0.5	0.4	885	183	55.3	19.2	13.9	9.0	6.2	4.5

3 Results

The results of the dose rate, obtained by the four codes, will be here described for the three scenarios introduced above: point source, area source and organ source. A comparative analysis of the results will be discussed later in Sect. 4.

3.1 Point sources

The values of the dose rate as a function of the distance from the point source were computed for Lu-177 and I-131 radionuclides (Fig. 4). For I-131, the dose rate was also calculated by using the equation given in IAEA1162 [21]. Since the differences between the dose profiles are not evident in the graph, for easier reading of data, we report in Table 3 the dose rate obtained at eight specific distances from the source (from 0.3 m to 3.5 m).

The curves of the deterministic methods complied with the inverse square distance law. From Table 3, the maximum deviation between RESRAD-BUILD and MicroShield was 5% regardless of the distance from the source, whereas the average deviation with MCNP6_photons was 6% (with a maximum deviation of 20%). The agreement between Geant4 and the results of the deterministic codes for distances greater than the extrapolated electron range from beta decays was within $\pm$ 10% (see Sect. 4 for discussion).

For distances close to the source, the dose rate calculated by Geant4 and MCNP6 is affected by the beta electron contribution. Although the beta contribution is not taken into account in the calculation with RESRAD-BUILD and MicroShield, it is here reported for completeness. The electron component of the dose rate is zeroed at a distance from the source of about 1.5 and 2.0 m for Lu-177 and I-131, respectively. This is close to the extrapolated range of betas for the maximum electron energy of about 497 keV (Lu-177) and 606 keV (I-131) [22]. In the curves by MCNP6 the electron component is zeroed at distances longer than Geant4. However, it is beyond the scope of the present work to investigate such a discrepancy.

3.2 Area sources (spill)

A spill of organic fluid (e.g., vomit, urine, blood) was simulated as an area disc-shaped source of water of 25 cm in diameter and 4 mm thick, positioned in the x–z plane of the reference system with the y-axis as the normal axis, perpendicular to the plane of the source and passing through its center as shown in Fig. 2.

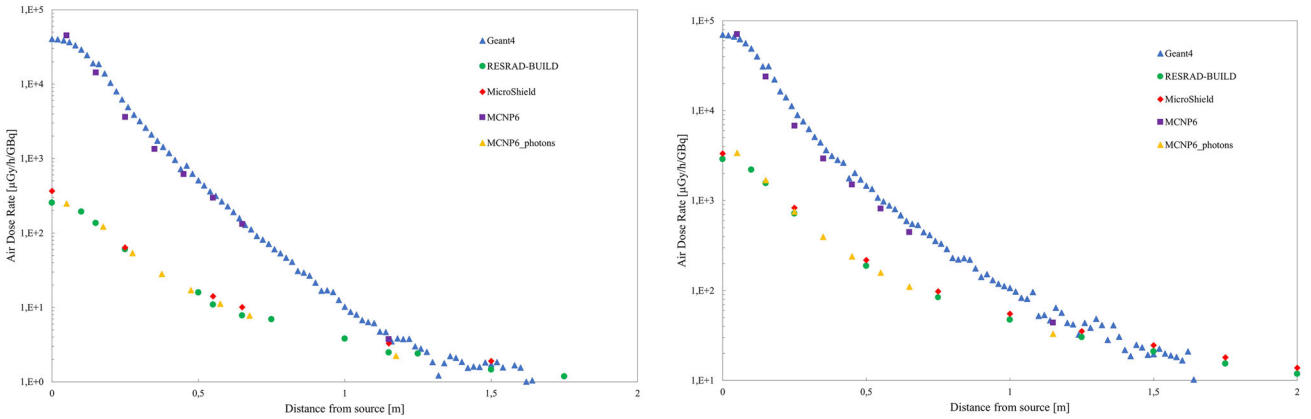

Fig. 5 Profile of the dose rate as a function of the distance from the center of the area source (spill of water) along the x-axis for Lu-177 (left) and I-131 (right). The dose rate was calculated along the x-axis at a fixed y-coordinate value of 10 cm

Table 4 Dose rate generated by the area source for Lu-177 and I-131

	Lu-177					I-131				
	0.25 m	0.55 m	0.65 m	1.15 m	1.5 m	0.25 m	0.55 m	0.65 m	1.15 m	1.5 m
Code	*Air dose rate (μGy/h/GBq)*									
Geant4	5543	337.4	143	4.08	1.72	10,058	1024.6	575.7	52.9	21.2
MCNP6	3617	296	132	3.7	–	6790	810	448		–
MCNP6_photons	54	11.2	7.8	2.2	–	749	158	110	33	–
RESRAD-BUILD	60.7	10.9	7.78	2.5	1.46	714	168	126	37.2	21
MicroShield	64	14.1	10.1	3.3	1.9	826	195	146	43.3	24.6

The dose rate was calculated along the x-axis with a fixed y-coordinate value of 10 cm. Distances are calculated from the y-axis passing through the center of the source

Table 5 Dose rate generated by the area source at five distances from the midpoint of the patient, for Lu-177 and I-131

	Lu-177					I-131				
	0.25 m	0.45 m	0.65 m	1.05 m	1.55 m	0.25 m	0.45 m	0.65 m	1.05 m	1.55 m
Code	*Air dose rate (μGy/h/GBq)*									
MCNP6	112.3	21.3	5.5	1.4	0.7	82.7	43.6	14.6	1.8	1.3
Geant4	145	28.7	7.3	1.7	0.9	113	62.9	21.5	4.4	2.4

The dose rate was calculated with Geant4 and MCNP6 along a line parallel to the x-axis and 0.1 m above the plane of the source, with the phantom placed between the source and the measurement point

The dose rate was calculated along the positive values of the x-axis with a fixed y-coordinate value of 10 cm (i.e., on a plane placed 10 cm above the plane of the source) (Fig. 5, left Lu-177, right I-131).

Table 4 shows the data for specific distances along x-axis (between 0.25 and 1.75 m).

In Fig. 5, the data appear to be divided into two groups, with the MCNP6 and Geant4 codes showing higher dose rate values than the deterministic dose rates, because of the contribution of electrons. The deterministic dose rate values are comparable to the results obtained by the MCNP6 code using only the photon energy spectrum (MCNP6_photons, in Fig. 5).

I-131 is known to induce nausea and vomiting in patients [23]. We then simulated a scenario with the area source on the bed, next to the patient. The scenario included the patient (with no radioactivity in the body) between the source and the measurement point to evaluate the difference in DRR due to radiation absorption or scattering from the patient's body (Fig. 6, Table 5). For this purpose, the same simulation of Fig. 5 was carried out for I-131 in the presence of a MIRD phantom, with the reference system centered in the phantom. The geometric center of the area source was placed 0.4 m from the phantom center along the x-axis (Fig. 3). The source was placed 0.1 m below the patient's midplane (along the y-axis), and the simulation was carried out along the x-axis passing through the patient's midplane.

The computed dose rates by Geant4 and MCNP6 for I-131 are shown in Fig. 6b. The sub-figure on the left shows the dose distribution in the x–z plane computed by Geant 4 for a view of the patient from the back, so that the spill image appears on the

right, in contrast to Fig. 3 where the patient was shown from the front. The sub-figure on the right shows the dose rate profiles. The dose rate at positive distances along x-axis is that already shown in Fig. 5, while the dose rate at negative distances is that affected by absorption by the patient's body. We then simulated a similar scenario for Lu-177, this time placing the spill with the same size, 0.4 m from the phantom center along the x-axis and 0.7 m below the patient's midplane (along the y-axis), to reproduce the accidental rupture of a urine bag on the floor, as shown in Fig. 6a, subfigure on the left. The effect of the absorbance from the phantom on the dose distribution can be appreciated by computing the dose rate on a line cutting the patient's midplane, that is 0.7 m above the spill. However, to investigate dose rate values at the same distance from the source along the y-axis as for I-131, values on a line 0.1 m above the spill have also been computed. The curves are shown in Fig. 6a.

On the negative abscissa in Fig. 6, and especially at distances greater than about 1 m, Geant4 shows a larger scatter than the results obtained on the side of the spill. This is due to the presence of the phantom, which renders the number of Geant4 simulated events insufficient at those distances from the source.

3.3 Organ sources

The third scenario involves the radionuclides being uniformly distributed in the organ of interest, using the MIRD phantom as the patient in Monte Carlo simulations. The organs considered are spleen, stomach and liver for Lu-177 and stomach and thyroid for I-131. Since the human body with deterministic codes can be modeled only by oversimplified geometries, this test has to be considered as a preliminary step to investigate this approach that we carried out only with RESRAD-BUILD. Figures 7 and 8 show the dose rate distributions for Lu-17 and I-131, respectively. The sub-figures on the left show a planar cross section of the volumetric

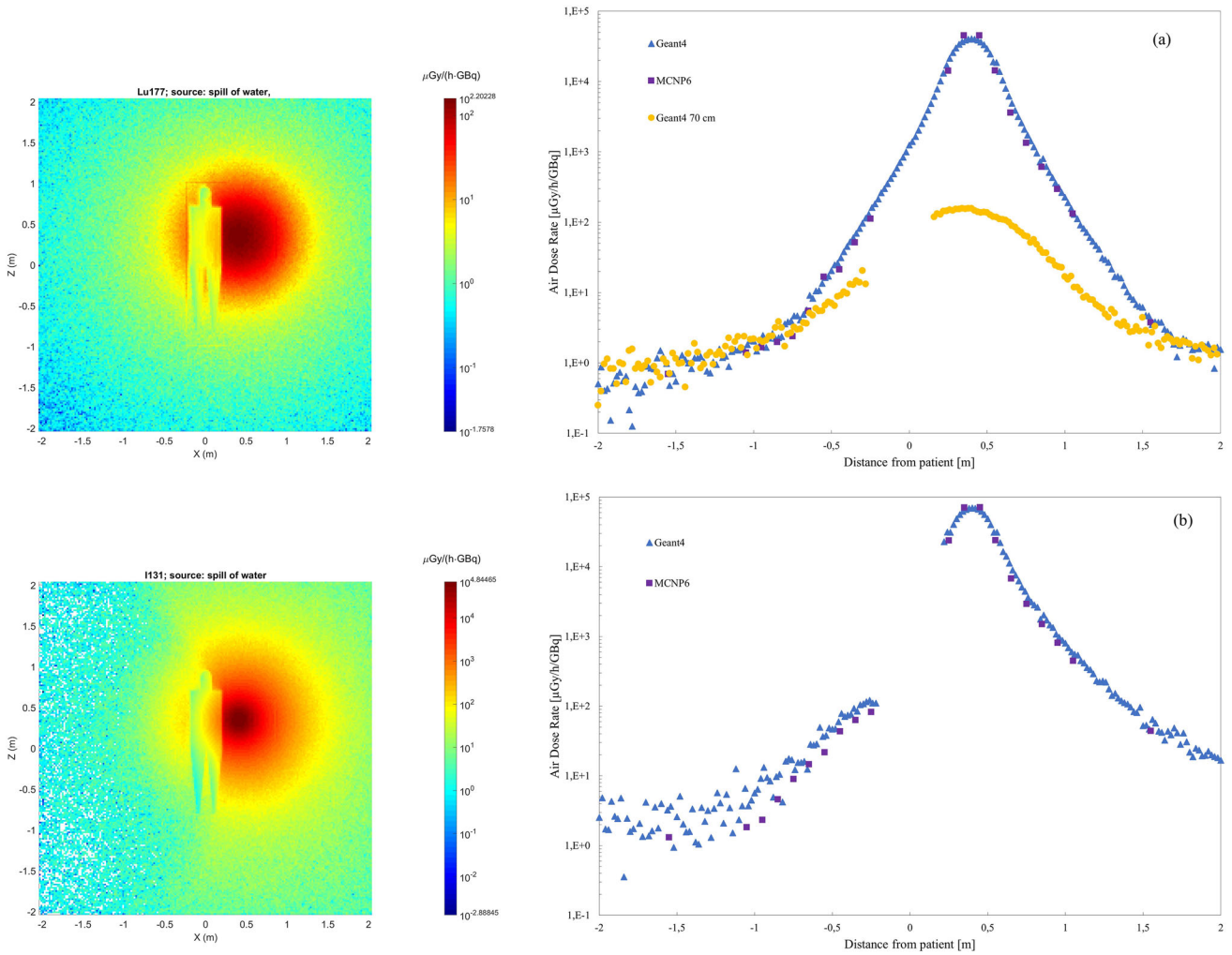

Fig. 6 Dose rate distribution on the x–z plane (left) calculated by Geant4 and dose rate profile along the x-axis (right) for Lu-177 (**a**) and I-131 (**b**) computed by Geant4 and MCNP6. The section of the dose distribution on the left was calculated at the patient's center plane. The dose rate profile for Lu-177 was computed at 0.1 m and at 0.7 m above the source plane, with 15,100 Mega primary particles for Geant4. The dose rate profile of I-131 was calculated at 0.1 m above the source plane with 800 Mega primary particles for Geant4. The distances along the x-axis are taken from the center y-axis of the patient

dose rate calculated with Geant4 and, as in the area source scenario, with a view of the patient from the back. The cross section was calculated at the level of the patient's center plane that is 0.7 m and 0.1 m above the source plane, for Lu-177 andI-131, respectively. The sub-figures on the right show the dose rate results of Geant4, MCNP6, RESRAD-BUILD and MicroShield, calculated along a line parallel to the x-axis, cutting the planar section along the highest dose value; the dose rate distribution curves are centered in the patient's axis center. For the sake of clarity, Tables 6 and 7 indicate the dose rate values for various distances from the patient, taken from the side where the organ is located (i.e., negative x-coordinates side for thyroid, stomach and spleen, positive x-coordinates side for liver).

All 2D dose rate distributions from Geant4 (Figs. 7 and 8, left) show areas where no dose was calculated; these areas are generally due to the phantom shield effect. To avoid this effect, it would be necessary to simulate a much larger number of primary events (or to consider larger voxels), requiring much greater computational resources, especially in terms of computing time. The figures on the right show the results obtained with Geant4 also inside the phantom. The 2 cm side of the voxels enables to appreciate the increase in the dose rate in areas close to the source.

4 Discussion

4.1 Analysis of the results of MCNP6 and Geant4

Before comparing the results of the Monte Carlo and the deterministic methods, we analyzed the dose rate calculated by Geant4 and by MCNP6 in the scenarios of point, area and organ sources.

For the point and the area sources, the electron component is the relevant contribution to dose rate when the distances are shorter than the extrapolated range of beta electrons. In this range, the calculated dose rate is higher for MCNP6 than for Geant4. Figure 9 shows DRR(r) of the Geant4 dose rate to the MCNP6 dose rate for the area source (data from Table 4). The error bars represent the combined uncertainty with coverage factor k = 1 [24]. In the graphs of Fig. 9, the Geant4 to MCNP6 DRR(r) was found to be between −17% and + 20%. The deviations of six out of eight points were within the combined uncertainty.

A general agreement within the combined uncertainty can be observed between the results of the two Monte Carlo simulations considering the MIRD phantom organs as sources (Fig. 10). Three distances from the center of the patient were considered, taken from the side where the organ is located in the body. As already mentioned, Geant4 statistics were found to be insufficient for high particle absorption, i.e., in the presence of higher body shielding. In addition, since Geant4 uses voxels of approximately 8 times smaller volume, chosen to obtain a higher-resolution image at higher dose rates, the scatter of the values is more pronounced in Geant4 simulations than in MCNP6. However, the agreement between MCNP6 and Geant4 is confirmed when the statistics in Geant4 are sufficiently high. This is the case of the water spill and the organ sources such as the spleen of Lu-177, Fig. 7a, and the thyroid and stomach simulation of I-131, Fig. 8.

It should be noted that Monte Carlo codes were used in this work as benchmarks of the deterministic codes and a comparison of the performances of Geant4 and MCNP6 codes was beyond the scope of the paper. Two Monte Carlo codes were chosen to complement each other in the different scenarios, as both were used with limitations in this work. For example, it was decided to use Geant4 with a high voxelization performed for the mixed electron and photon field. On the other hand, MCNP6 was more stable, but the measurement volume was larger. The electron and photon components were treated separately. The above but, for reasons of computational time, with a number of histories which, in a few cases, did not give a stable response. Furthermore, Geant4 was only analysis of the Monte Carlo codes was then finalized to exclude significant systematic biases generated by the chosen computational models and to decide under which conditions to use one or the other code to verify the results of the deterministic codes.

4.2 Analysis of the results of the deterministic codes against Monte Carlo codes

In the point-source model (Fig. 4 and Table 3), the mean value of the DRR(r) determined by RESRAD-BUILD to MicroShield for distances from 0.25 m to 3.5 m was 1.01 ± 0.04 for Lu-177 and 0.99 ± 0.04 for I-131. The mean value of DRR(r) determined by RESRAD-BUILD to MCNP6_photons was higher than 1; in particular, it was 1.19 ± 0.06 for Lu-177 and 1.09 ± 0.07 for I-131; similarly, the DRR(r) of MicroShield to MCNP6_photons was 1.17 ± 0.03 for Lu-177 and 1.10 ± 0.04 for I-131. The dose rate values calculated by Geant4 for distances shorter than 0.5 m were about three orders of magnitude higher than those calculated by the deterministic codes, and then dropped to similar values at distances of 1.5 to 2 m, as expected because the deterministic codes are only sensitive to the photonic fraction.

For the area source, Fig. 11 shows the DRR(r) of RESRAD-BUILD and MicroShield to MCNP6_photons for Lu-177 (left) and I-131 (right). The mean values between 0.25 m and 1.15 m of DRR(r) values were: 1.13 ± 0.17 (Lu-177) and 1.02 ± 0.14 (I-131) for MicroShield to MCNP6_photons and 0.90 ± 0.07 (Lu-177) and 0.88 ± 0.12 (I-131) for RESRAD-BUILD to MCNP6_photons. It is to be noted that MicroShield results regarding Lu-177 isotope are systematically higher (within 23%) than those computed by RESRAD-BUILD and MCNP6_photons. Similar results are reported in literature [10, 25] and are probably due to the methods MicroShield uses to compute attenuation and build-up factors in air. The differences between the deterministic codes could also be due to additional aspects, including: the RESRAD-BUILD approximations for the radionuclide's energy spectrum; the interpolation

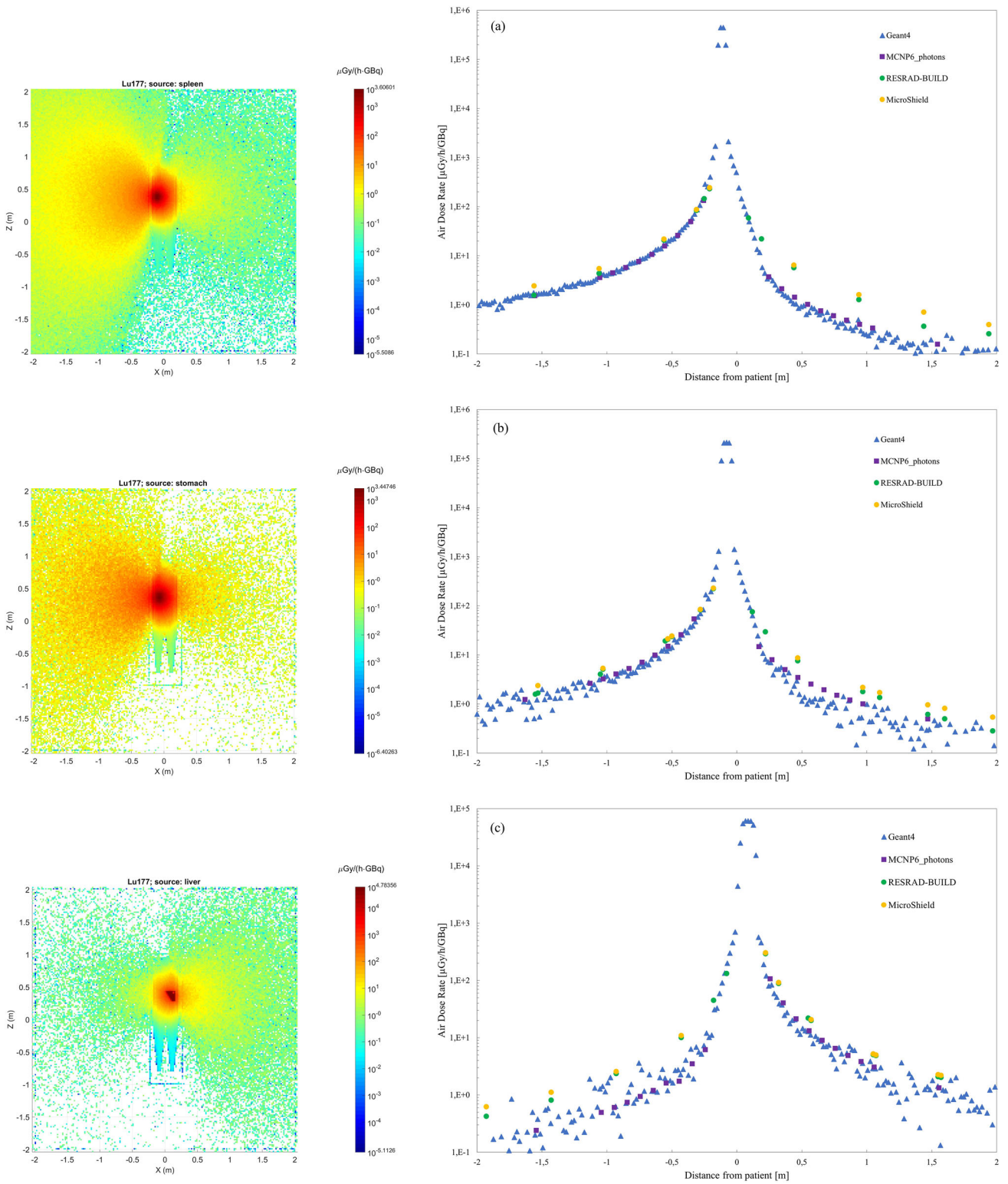

Fig. 7 Dose rate distribution on the x–z plane (left) computed by Geant4 and dose rate profile along the x-axis (right) for Lu-177 computed by Geant4, MCNP6_photons, RESRAD-BUILD and MicroShield for three organs as a source of Lu-177: **a** spleen (Geant4 used 21,080 Mega primary particles); **b** stomach (3000 Mega primary particles); **c** liver (2000 Mega primary particles). The section of the dose distribution on the left was calculated at the patient's center plane. For the dose rate profiles on the right, the distances along the x-axis are taken from the patient's axis center. The rectangular shape in the dose distributions (left) is due to a computational artifact at the border between the box containing the phantom and the outer space

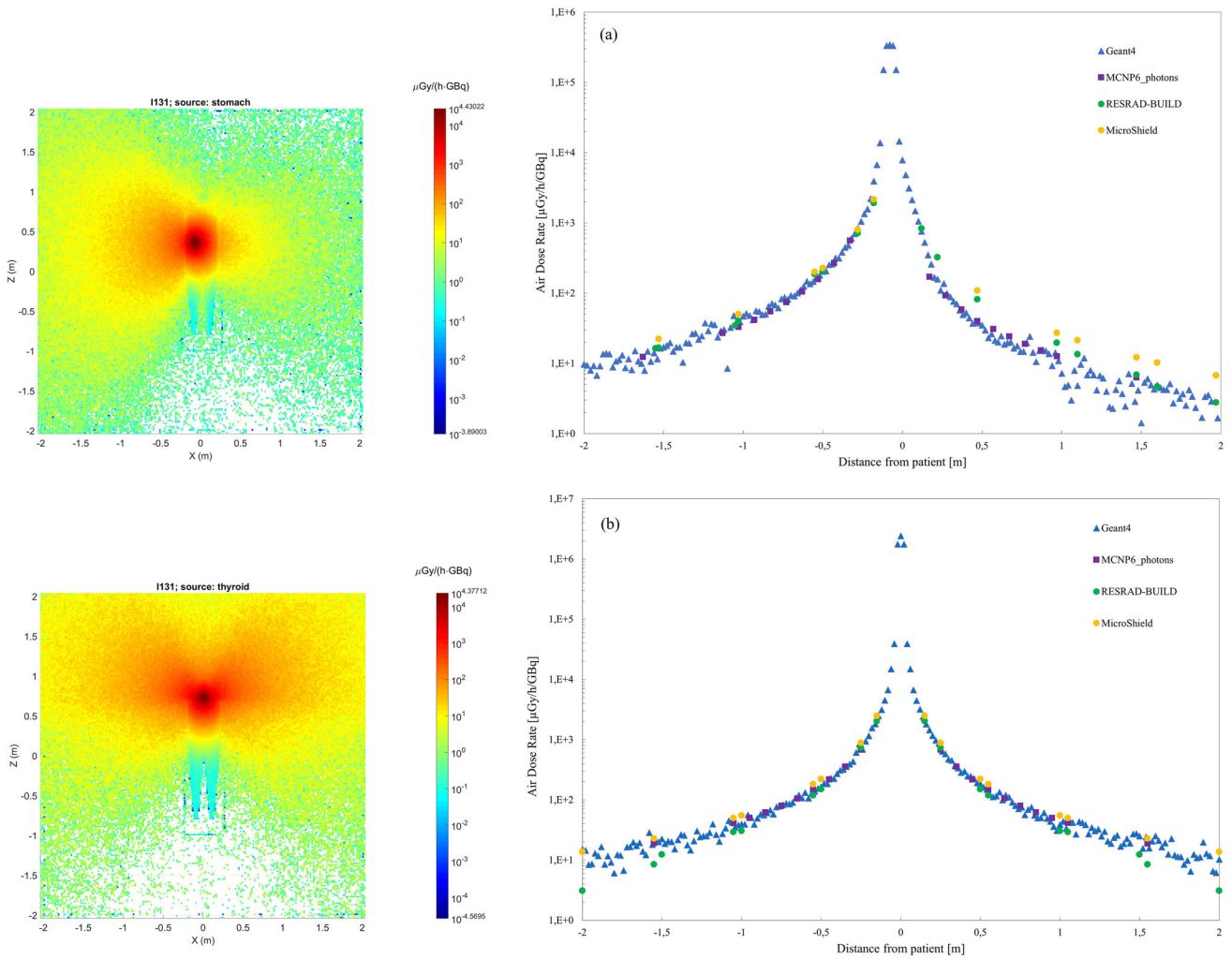

Fig. 8 Dose rate distribution on the x–z plane (left) computed by Geant4 and dose rate profile along the x-axis (right) for I-131 computed by Geant4, MCNP6_photons, RESRAD-BUILD and MicroShield for two organs as a source of I-131: **a** stomach (Geant4 used 800 Mega primary particles); **b** thyroid (800 Mega primary particles). The rectangular shape in the dose distributions (left) is due to a computational artifact at the border between the box containing the phantom and the outer space

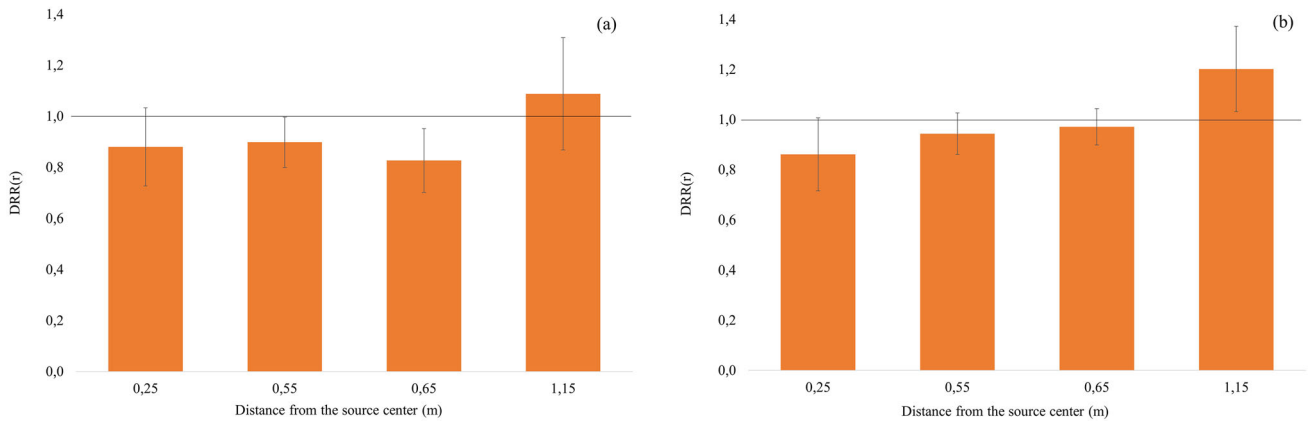

Fig. 9 Geant4 dose rate to MCNP6 dose rate ratio with distance along the x-axis from the center of the area source, for Lu-177 **a** and I-131 **b**. The error bar represents the combined uncertainty with coverage factor k = 1

of point-kernel results for dose estimate in RESRAD-BUILD against the direct application of a traditional point-kernel method as in MicroShield; and the usage of conversion factors from effective dose to air dose in RESRAD-BUILD, whose uncertainty and

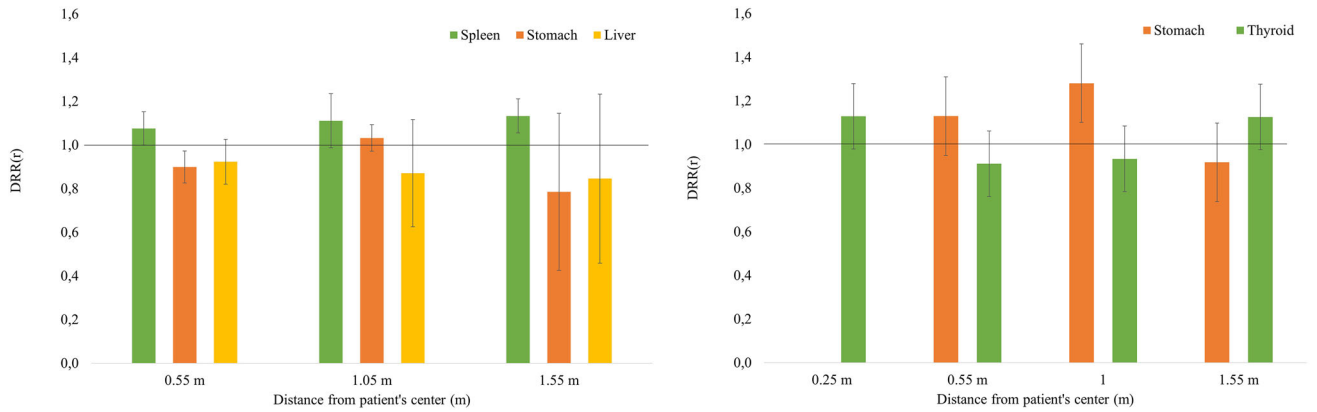

Fig. 10 Ratio of Geant4 dose rate to MCNP6 dose rate from the activity on the organs, as a function of the distance from the patient's center for Lu-177 (left) and I-131 (right). The error bar is the combined uncertainty

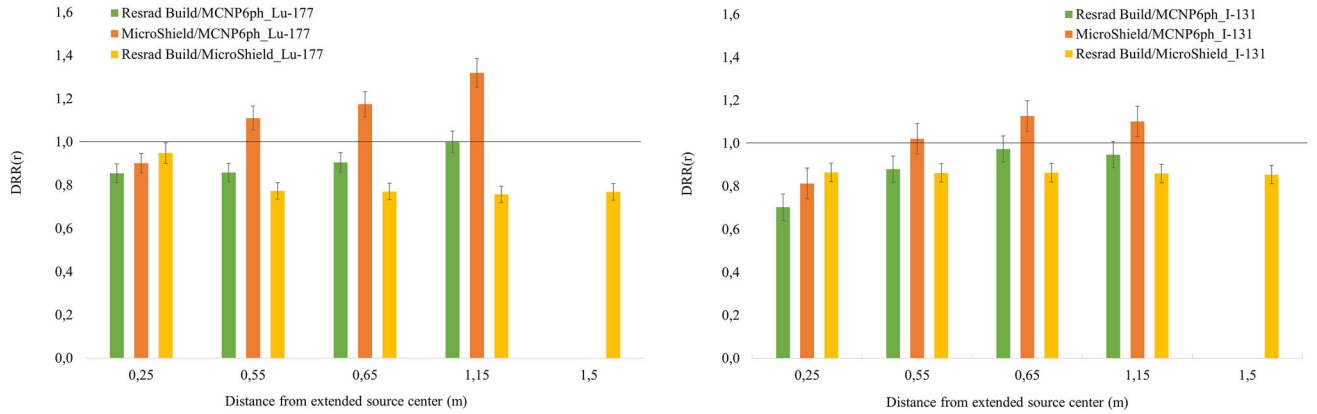

Fig. 11 Ratio of RESRAD-BUILD and MicroShield dose rate to MCNP6_photons dose rate, as a distance from the area source center, for Lu-177 (left) and I-131 (right). The error bar is the combined uncertainty. The ratio of the RESRAD-BUILD to MicroShield dose rate is also shown

value depend on the energy (uncertainty from 2.5% to 15% for energy less 30 keV). It is worth to note that the conversion factors are calculated for monoenergetic energy value; for broad spectrum energy, they should be calculated by integration over the whole spectrum, and in presence of mixed electron and photon radiation field, they should be calculated adding the respective single contributions [18].

Finally, in Fig. 12 we discuss the comparison between the DRR(r) of RESRAD-BUILD to MCNP6_photons with the organs of the MIRD phantom as sources, considering three distances from the patient's center, taken from the side where the organ is located in the body (the data are shown in Figs. 7 and 8 and Table 6, 7). The deviations, averaged over organs and distance (Fig. 12), between RESRAD-BUILD and MCNP6_photons were 1.3 ± 0.22 for Lu-177 and 0.89 ± 0.25 for I-131. This can be assumed as an acceptable value considering the simplification of the organs carried out in RESRAD-BUILD, where the organs were simulated as parallelepipeds surrounded by other simple geometries of watery materials to reconstruct the lateral dimensions of the MIRD phantom. For the liver, the deviations between RESRAD-BUILD and MCNP6_photons dose rate were about 60%, probably due to the complexity of the organ geometry, not easily to be modeled with the regular shapes allowed by the code. The dose rate from the thyroid shows a tendency to decrease more rapidly, especially at longer distances. This is an unexpected result because the thyroid is a relatively easy organ to simulate even with simplified geometries such as those of RESRAD-BUILD, the shielding effect of the body (actually the neck) is small. This could be probably due to a change in the area factors used by RESRAD-BUILD to compute the dose for finite sources as distance grows, due to the small thickness of the thyroid. An improvement would be a more refined description of the volume sources, leading to a more accurate description of the geometry of the organ. When looking at the results by MicroShield, the mean value over organs and distance of MicroShield to MCNP6_photons DRR (r) was 1.60 ± 0.13 for Lu-177 and 1.34 ± 0.13 for I-131, confirming the systematic deviation of about 30% between RESRAD-BUILD and MicroShield.

On the opposite side of the organ in MIRD phantom in Fig. 7a and c, corresponding to the spleen and liver scenarios at Lu-177, the dose rate is significantly larger for RESRAD-BUILD than for MCNP6, probably for the limits of RESRAD-BUILD to reproduce the absorption of the body around organs centered further from the patient's axis.

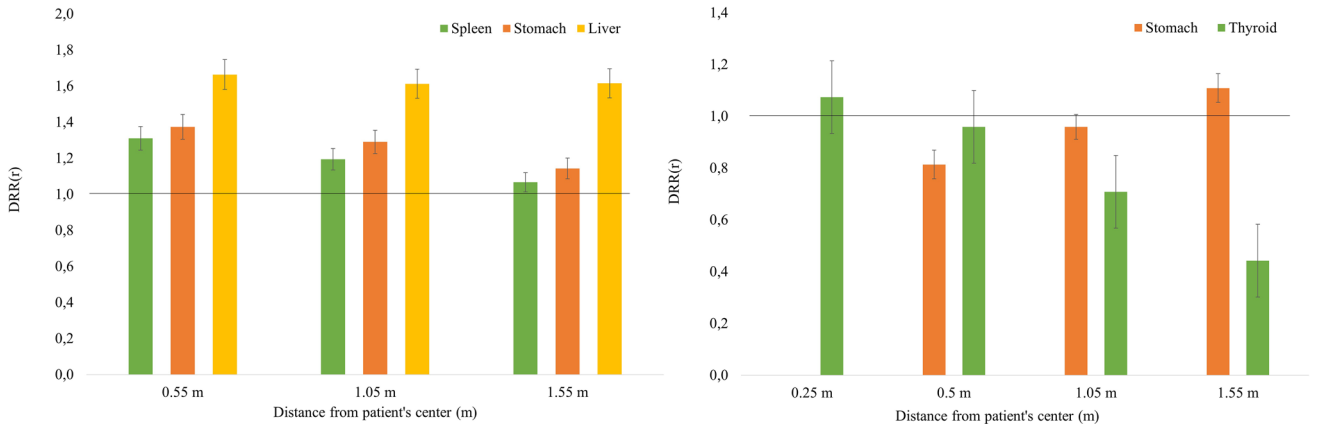

Fig. 12 Ratio of RESRAD-BUILD dose rate to MCNP6_photons dose rate, as a function of the distance from the patient's center for Lu-177 (left) and I-131 (right). The error bar is the combined uncertainty

Table 6 Comparison dose rate data for three Lu-177 organ sources: spleen, liver and stomach

	0.55 m			1.05 m			1.55 m		
	Spleen	Stomach	Liver	Spleen	Stomach	Liver	Spleen	Stomach	Liver
Code	*Air dose rate (μGy/h/GBq)*								
MCNP6	15.8	13.9	13.1	3.6	3.1	3.1	1.5	1.4	1.3
Geant4	17	12.5	12.1	4	3.2	2.7	1.7	1.1	1.1
RESRAD-BUILD	20.7	19.1	21.8	4.3	4	5	1.6	1.6	2.1
MicroShield	21.8	20.3	22.5	5.4	5.2	5.2	2.4	2.3	2.3

Table 7 Comparison dose rate data for two I-131 organ sources: thyroid and stomach

	0.25 m	0.55 m		1.05 m		1.55 m	
	Thyroid	Stomach	Thyroid	Stomach	Thyroid	Stomach	Thyroid
Code	*Air dose rate (μGy/h/GBq)*						
MCNP6	679	146.7	146	31.7	41.1	14.7	19
Geant4	767	165.8	133.2	40.6	38.4	13.5	21.4
RESRAD-BUILD	729	162.9	118.8	30.4	29.1	16.3	8.4
MicroShield	881	200	181	49.2	50	21.6	23

5 Conclusions

New opportunities for real-time dosimetry for workers are offered by advanced computational dosimetry and computer vision methods, especially when conventional dosimetry is inadequate.

The accurate approaches based on Monte Carlo techniques are demanding on computing time and difficult to use for non-experts. The faster although less accurate deterministic methods might be an alternative when radiation maps need to be created in a short time, for instance in the occurrence of small accidents in nuclear medicine therapy rooms, as the ones described in the present work.

By using Monte Carlo simulation as benchmark, we analyzed the results of two deterministic codes (RESRAD-BUILD and MicroShield) in scenarios of small accidents likely to occur in nuclear medicine therapy rooms with Lu-177 and I-131 radionuclides. In all scenarios, the maximum deviation of the dose rate between the deterministic codes was within 4% for the point source and within 25% for the area source and within $\pm$ 15% when compared to the Monte Carlo codes. Considering that the scope is to estimate the external dose to workers in accidental situations, an uncertainty of this order is acceptable and comparable to the uncertainty in conventional personal dosimetry. It is interesting to note that the simplified simulation of the organs carried out by RESRAD-BUILD was in sufficient agreement (within 40%) with the more refined Monte Carlo simulations performed with the MIRD phantom.

There is clearly room for improvement in simulation by the deterministic codes, as highlighted in the paper. The study could be improved by increasing the number of histories in the Monte Carlo computations and by making the geometry of the volume sources more refined in the deterministic codes.

Authors' contribution GS and PF conceived and planned the experiments. GS, CA, GV, CN and PF planned, carried out and interpreted the results of the simulations. GS, PF, CA, CZ performed the comparative analysis, and GS, PF, CZ took the lead in writing the manuscript in consultation with all Authors. All authors provided critical feedback and helped shape the research, analysis and manuscript.

Funding The SIREN project is funded by the Activity Plan for Scientific Research 2019–2021 of the Italian National Institute for Insurance against Accidents at Work (INAIL), grant BRIC 2019, themes ID n.44/2019.

Data availability statement The datasets generated during and/or analyzed during the current study are available from the corresponding author or the first author on reasonable request.

Declarations

Conflict of interest The authors declare that they have no conflicting interests.

References

1. F. Vanhavere, O. Van Hoey. Advances in personal dosimetry towards real-time dosimetry. Radiat. Meas. **158**, 106862 (2022). https://doi.org/10.1016/j.radmeas.2022.106862
2. A. Almén, M. Andersson, U. O'Connor, M. Abdelrahman, A. Camp, V. García, M.A. Duch, M. Ginjaume, F. Vanhavere, Personal dosimetry using monte-carlo simulations for occupational dose monitoring in interventional radiology: the results of a proof of concept in a clinical setting. Radiat. Prot. Dosimetry **195**(3–4), 391–398 (2021). https://doi.org/10.1093/rpd/ncab045.PMID:33823548;PMCID:PMC8507461
3. T. Tsujiguchi, Y. Suzuki, M. Sakamoto et al., Simulation study on radiation exposure of emergency medical responders from radioactively contaminated patients. Sci. Rep. **11**, 6162 (2021). https://doi.org/10.1038/s41598-021-85635-2
4. H. Han, YS. Yeom, C. Choi et al. Dose coefficients for use in rapid dose estimation in industrial radiography accidents. In S. Makarov et al. (eds.), Brain and Human Body Modeling at EMBC 2018 (Springer, 2019), pp. 295–304. https://doi.org/10.1007/978-3-030-21293-3_15
5. G. Stendardo, C. Nuccetelli, S. Grande, A. Palma, G. Venoso, C. Zicari, C. Andenna, G. Frau, I. Bonanno, V. Landoni, R. Sciuto, V. Bruzzaniti, B. Cassano, G. Iaccarino, F. Murtas, C. Canzi, F. Zito, P. Fattibene, A real-time system to report abnormal events involving staff in a nuclear medicine therapy unit. Radiat. Prot. Dosim. **199**(8–9), 962–969 (2023). https://doi.org/10.1093/rpd/ncad098
6. C. Canzi, G. Stendardo, S. Grande, C. Nuccetelli, A. Palma, C. Zicari, C. Andenna, G. Frau, T. Vendruscolo, V. Landoni, F. Murtas, R. Sciuto, V. Bruzzaniti, B. Cassano, G. Iaccarino, F. Zito, G. Venoso, P. Ferrari, P. Fattibene, PC-07.2 - an internet of things (iot) system to report on abnormal events in nuclear medicine therapy patient rooms. Physica Medica, Vol. **115**, Supplement 1, 2023, 102950, ISSN 1120–1797, https://doi.org/10.1016/j.ejmp.2023.102950.
7. RESRAD Family of Codes. https://resrad.evs.anl.gov/. Accessed 31 july 2023.
8. MicroShield® User's Manual Version 12. Grove Software, Inc. (2019). https://radiationsoftware.com/microshield. Accessed 31 July 2023.
9. C. Yu, J.-J. Cheng, E. Gnanapragasam, S. Kamboj, D. LePoire, and C. Wang. User's manual for RESRAD-BUILD code V.4: Vol. 1—methodology and models used in RESRAD-BUILD code. United States (2022). https://doi.org/10.2172/1906354
10. A.D. Oliveira, C. Oliveira, Comparison of deterministic and Monte Carlo methods in shielding design. Radiat. Prot. Dosim. **115**(1–4), 254–257 (2005). https://doi.org/10.1093/rpd/nci187
11. D. Bednár, M. Ličtjak, A. Slimák, V. Nečas, Comparison of deterministic and stochastic methods for external gamma dose rate calculation in the decommissioning of nuclear power plants. Ann. Nucl. Energy **134**, 67–76 (2019). https://doi.org/10.1016/j.anucene.2019.06.003
12. S.K. Gupta, S. Singla, P. Thakral, C.S. Bal, Dosimetric analyses of kidneys, liver, spleen, pituitary gland, and neuroendocrine tumors of patients treated with 177Lu-DOTATATE. Clin. Nucl. Med. **38**(3), 188–194 (2013). https://doi.org/10.1097/RLU.0b013e3182814ac1
13. C.C. Huang, Y.H. Lin, S. Kittipayak, Y.S. Hwua, S.Y. Wang, L.K. Pan, Biokinetic model of radioiodine I-131 in nine thyroid cancer patients subjected to in-vivo gamma camera scanning: a simplified five-compartmental model. PLoS ONE **15**(5), e0232480 (2020). https://doi.org/10.1371/journal.pone.0232480
14. Accelerators, Spectrometers,J. Allison, et al., Recent developments in Geant4. Nucl. Instrum. Methods Phys. Res. Sect. A Detectors Assoc. Equip. **835**, 186–225 (2016). https://doi.org/10.1016/j.nima.2016.06.125
15. J. Allison et al., Geant4 developments and applications. IEEE Trans. Nucl. Sci. **5**(1), 270–278 (2006). https://doi.org/10.1109/TNS.2006.869826
16. S. Agostinelli et al. Geant4—a simulation toolkit. Nucl. Instrum. Methods Phys. Res. Sect. A Accelerators Spectrometers Detectors Assoc. Equip., **506**(3): 250–303. https://doi.org/10.1016/S0168-9002(03)01368-8
17. J. A. Kulesza (Editor), MCNP® Code Version 6.3.0 Theory & User Manual, Los Alamos National Laboratory, LA-UR-22–30006, Rev. 1 (2022)
18. Conversion Coefficients for use in Radiological Protection against External Radiation. ICRP Publication 74. Ann. ICRP 26 (3–4) (1996).
19. Conversion Coefficients for Radiological Protection Quantities for External Radiation Exposures. ICRP Publication 116, Ann. ICRP 40 (2–5) (2010).
20. Nuclear Decay Data for Dosimetric Calculations. ICRP Publication 107. Ann. ICRP 38 (3) (2008).
21. INTERNATIONAL ATOMIC ENERGY AGENCY, *Generic procedures for assessment and response during a radiological emergency, IAEA-TECDOC-1162* (IAEA, Vienna, 2000)
22. M. Pelliccioni, Fondamenti fisici della radioprotezione, Ed. Pitagora (1993).
23. M. Pashnehsaz, A. Takavar, S. Izadyar, S.S. Zakariaee, M. Mahmoudi, R. Paydar, P. Geramifar, Gastrointestinal side effects of the radioiodine therapy for the patients with differentiated thyroid carcinoma two days after prescription. World J. Nucl. Med. **15**(3), 173–178 (2016). https://doi.org/10.4103/1450-1147.174703
24. ISO/IEC Guide 98–3:2008 Uncertainty of measurement. Part 3: Guide to the expression of uncertainty in measurement (GUM:1995)

25. Tetra Tech NUS, Inc. Verification of RESRAD-BUILD Computer Code, Version 3.1, prepared for Argonne National Laboratory under Contract No. 1F-00741. (2003)